Bonding, Backbonding, and Spin-Polarized Molecular Orbitals: Basis for Magnetism and Semiconducting Transport in V[TCNE]$_{x\sim2}$

J. B. Kortright,[1] D. M. Lincoln,[3] R. Shima Edelstein,[2] and A. J. Epstein[2,3]

[1]*Materials Sciences Division, Lawrence Berkeley National Laboratory, Berkeley, California 94720-8099, USA*
[2]*Department of Physics, The Ohio State University, Columbus, Ohio 43210-1117, USA*
[3]*Department of Chemistry, The Ohio State University, Columbus, Ohio 43210-1185, USA*

(Received 20 February 2008; published 27 June 2008)

X-ray absorption spectroscopy (XAS) and magnetic circular dichroism (MCD) at the V $L_{2,3}$ and C and N K edges reveal bonding and backbonding interactions in films of the 400 K magnetic semiconductor V[TCNE]$_{x\sim2}$. In V spectra, d_{xy}-like orbitals are modeled assuming V^{2+} in an octahedral ligand field, while d_{z^2} and $d_{x^2-y^2}$ orbitals involved in strong covalent σ bonding cannot be modeled by atomic calculations. C and N MCD, and differences in XAS from neutral TCNE molecules, reveal spin-polarized molecular orbitals in V[TCNE]$_{x\sim2}$ associated with weaker π bonding interactions that yield its novel properties.

DOI: 10.1103/PhysRevLett.100.257204 PACS numbers: 75.50.Xx, 61.05.cj, 75.50.Pp, 78.20.Ls

Vanadium tetracyanoethylene (V[TCNE]$_{x\sim2}$) stands out in a broader class of condensed phase, molecule-based magnets [1,2] by exhibiting magnetic ordering to 400 K [3], semiconducting magnetoresistive transport [4,5], and photoinduced magnetism [6,7]. These novel properties imply a distinct, spin-polarized electronic structure [4], but its details have remained elusive. While a nominal structural model for short-range order in V[TCNE]$_{x\sim2}$ has emerged [8], inherent structural disorder and metastability of both solution prepared powders [3] and solvent free chemical vapor deposition (CVD) films [9] have hindered thorough understanding of the electronic structure underlying its properties. The nominal structural model is based on a simple ionic picture with spin $S = 3/2$ V^{2+} coordinating octahedrally with 1 of the 4 N terminations of 6 different $S = 1/2$ $TCNE^{\bullet-}$ radical anion ligands. Long-range crystalline order is absent and the structure is networklike with $TCNE^{\bullet-}$ bridging V^{2+}, and vice versa. For $x = 2$ only 3/4, on average, of the N of each $TCNE^{\bullet-}$ coordinate with V^{2+} to maintain charge neutrality. Recent V K edge EXAFS supports this model, yielding 6 N atoms at 2.08 Å from the central V^{2+} [8].

Several studies aim to elucidate this electronic structure. Photoemission spectroscopy of Rb intercalated TCNE [10] and V[TCNE]$_x$ [11,12] shows metal-induced changes in TCNE valence states. X-ray absorption (XAS) and magnetic circular dichroism (MCD) spectroscopy at the V $L_{2,3}$ edges of V[TCNE]$_x$ [11,12] were partially modeled by atomic multiplet calculations [12]. These studies were interpreted to imply strong but unspecified covalent bonding between V and TCNE with V in a mixed-valent, charge-transfer ground state consisting of $V^{2+} + V^{1+}L$ where L is a ligand hole on TCNE. While these studies advance knowledge of V[TCNE]$_{x\sim2}$, they leave important aspects of the V XAS spectra unexplained, do not provide a specific covalent bonding mechanism, and do not explore the role of TCNE in the spin-resolved electronic properties.

In this Letter, we report XAS and MCD measurements at the V $L_{2,3}$ and C and N K edges in V[TCNE]$_{x\sim2}$ films and the C and N edges in isolated TCNE molecules. Our V results reveal additional features compared to previous studies, leading to a very different interpretation. At the C and N edges we observe changes in the molecular orbital (MO) structure of TCNE in V[TCNE]$_{x\sim2}$ films compared to gas-phase TCNE, including spin-polarized states near the Fermi level (E_F). Combined results reveal interactions between V d states and TCNE MO states involving strong covalent σ bonding and weaker, spin-polarized π backbonding.

V[TCNE]$_{x\sim2}$ films (100–200 nm thick) were deposited by CVD [9] onto SiN_x membrane substrates (100 nm thick), capped with Al (30 nm) to suppress oxidation, and sealed in evacuated ampoules. At the Advanced Light Source samples were removed in N_2 and introduced into the vacuum chamber with minimal air exposure. O K edge XAS revealed that some samples contained observable O. Data reported here, however, are from samples showing no trace of O by XAS [Fig. 1(a)]. XAS and MCD were measured in transmission at 298 K with circularly polarized x rays (degree of circular polarization ~0.85). An electromagnet applied an ac field (5 Hz, +/− 200 Oe peak) to facilitate lock-in detection of weak MCD at the C and N edges. Fixed helicity MCD features change sign on helicity reversal proving they are real. C and N XAS were also measured from gas-phase, neutral TCNE ($TCNE^0$) for comparison with films.

Vanadium XAS [Fig. 1(b)] resolves at least 4 L_3 multiplet peaks and 2 L_2 peaks, indicating that a predominant V charge state and ligand field environment exist in V[TCNE]$_{x\sim2}$. This structure is similar to, but more pronounced than, that in Ref. [12]. Using atomic ligand field multiplet (LFM) calculations ($T = 0$ K) we evaluated V^{n+} spectra for $n = 1$–3 in an octahedral ligand field (O_h) of varying strength $10Dq$ [13]. The best result [Fig. 1(b)] is

 © 2008 The American Physical Society

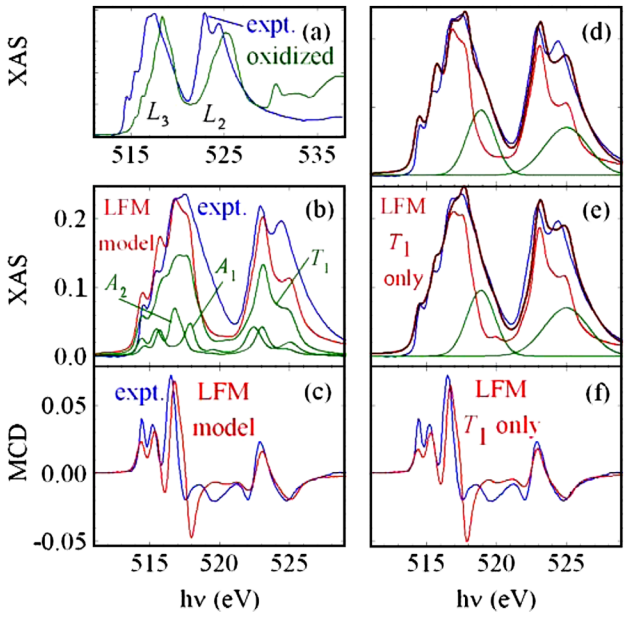

FIG. 1 (color online). Measured V $L_{2,3}$ edge XAS and MCD (blue or dark gray). (a) compares XAS from an intentionally oxidized sample (green or light gray) with a fresh sample. (b) and (c) show calculated XAS and MCD for a full LFM model assuming V^{2+} in O_h with $10Dq = 2.4$ eV. The same vertical scaling factor has been applied to both XAS and MCD spectra. In (d) the model (dark red or gray) is the sum of the same LFM spectrum and two Gaussians shown (green or light gray). (e) and (f) include just the T_1 component of an LFM model with $10Dq = 2.25$ eV.

for V^{2+} ($d3$), consistent with expectations [9,12], with $10Dq = 2.4$ eV. Model spectra are broadened by a Gaussian of width 0.2 eV to simulate experimental resolution, by Lorentzians of width 0.2(0.4) eV in the $L_3(L_2)$ regions to simulate lifetime broadening, and a Fano line shape asymmetrically broadens the L_2 line to simulate interference between $2p_{1/2}$ and $2p_{3/2}$ channels. While multiplets at the leading edge of both L_3 and L_2 lines are reproduced, significant intensity not reproduced broadens measured lines to higher energy. This extra broadening was observed but not modeled in Ref. [12]. We find that one broad Gaussian at each L_3 and L_2 line added to the LFM model accounts for all features and the entire width of the spectrum [Fig. 1(d)]. These Gaussians account for 27% of the total XAS intensity of this new model.

The significance of these *ad hoc* Gaussians is of central importance, and not obvious *a priori*. Within LFM theory they could result as simple admixtures of different charge states or from charge transfer to or from ligands yielding different charge states that mix before evaluation of the dipole transition matrix element [13]. Indeed the Gaussians are located where V^{3+} multiplet structure would exist. We explored and do not adopt these models for several reasons. An added V^{3+} contribution would have its own multiplet structure that is not apparent in the data. Charge-transfer models result in narrower multiplet lines compared to simple LFM models of comparable $10Dq$ [13] and cannot model the full spectral breadth. The sharp distribution of N about V^{2+} from V K EXAFS [8] is inconsistent with multiple valence states. The Gaussians are too large to be excited state satellites. We propose instead that they result from covalent bonding between V and TCNE that atomic multiplet theory cannot describe, and develop a covalent bonding model consistent with V, C, and N XAS.

Covalent bonding is expected in organometallic molecules in which octahedrally coordinated transition metal ions interact with ligands through distinct σ bonding and π backbonding mechanisms. Aspects of this model have been considered for nonmagnetic molecules containing V^{2+} [14] and for crystalline hexacyanometalate magnets [15,16]. To investigate applicability of this general model to $V[TCNE]_{x\sim2}$, note that the V^{2+} LFM spectrum in Fig. 1(b) decomposes into 3 final state resolved symmetries [13]; threefold degenerate T_1 states describe transitions into the d_{xy}, d_{xz}, and d_{yz} orbitals while onefold A_1 and A_2 states describe transitions into the d_{z^2} and $d_{x^2-y^2}$ orbitals and account for 33% of the XAS intensity. Hybridization associated with strong covalent σ bonding would redistribute d_{z^2} and $d_{x^2-y^2}$ states into bonding and antibonding states not describable by atomic theory. Weaker π interactions, however, might yield T_1 contributions approximated by LFM models. Indeed the T_1 spectrum itself approximates that measured with $10Dq = 2.25$ eV [Fig. 1(e)]. The same Gaussians added to this T_1 spectrum yield a good approximation of the V XAS, where now they are identified with transitions into empty A_1 and A_2 states hybridized into σ^* states $\sim$5 eV above E_F. This is consistent with covalent σ bonding between d_{z^2} and $d_{x^2-y^2}$ states and the lone pair electrons localized in $TCNE^{\bullet-}$ σ MOs, and much weaker interaction between the T_1 states and the $TCNE^{\bullet-}$ π MO system.

V MCD data are modeled equally well by the full V^{2+} LFM model [Fig. 1(c)] and the T_1-only LFM model [Fig. 1(f)]. Calculations reveal that transitions into T_1 states account for all MCD at $T = 0$ K and most MCD at 300 K. Even without sum rule analysis to separate spin (m_s) from orbital (m_l) moments [17,18], the comparable size of measured and model MCD confirms that V^{2+} is essentially fully spin polarized in a high-spin configuration ($m_s = 3, S = 3/2$) key to the high T_C of $V[TCNE]_{x\sim2}$. The ratio $m_l/m_s \cong -0.01$, with m_l opposing m_s as expected by Hund's rules.

XAS at the C and N K edges of $TCNE^0$ reveals a well-defined MO structure with 3 π^* peaks in each spectrum (Fig. 2) representing transitions from localized $1s$ atomic levels into the 3 lowest unoccupied MO (LUMO) states having characteristic empty density of states (DOS) distributions extending across the molecule [19–21]. C and N spectra probe the 3 LUMOs from different sites within the molecule. The first peak results from transitions to the lowest π^* MO with DOS antinodes out of the molecular plane and lobes localized near the central C_1 and the N

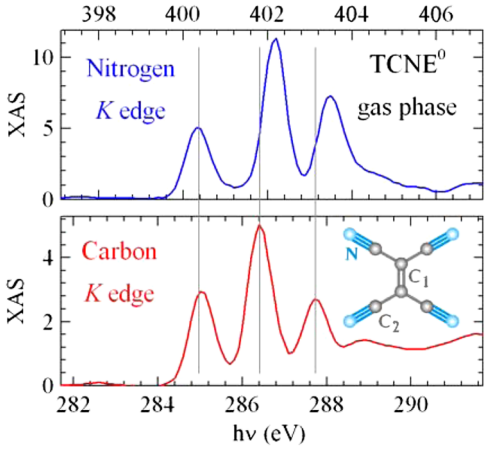

FIG. 2 (color online). C and N XAS of $TCNE^0$. Energy scales align the first peaks and each spectrum spans 10 eV. Vertical lines are visual guides. Ball and stick model of $TCNE^0$ (inset).

sites (Fig. 2 inset). The second and third peaks result from transitions to 2 π^* MO states associated more with the $C_2 \equiv N$ triple bonds. The splitting between the first and second peaks differs at the C and N edges, while that between the second and third peaks is identical; this results from different screening of C_1 and C_2 sites contributing to the first and to the second and third peaks, respectively.

C and N XAS spectra of $V[TCNE]_{x\sim2}$ show significant similarities and differences compared to those of $TCNE^0$ [Figs. 3(a) and 3(b)]. The $TCNE^0$ second and third LUMO peaks remain intact, albeit significantly broadened, in $V[TCNE]_{x\sim2}$. The first LUMO in the C spectra splits into two peaks, while three peaks can be resolved in the low energy region of the N spectra. We measure reduction in C and N π^* density in $V[TCNE]_{x\sim2}$ compared to $TCNE^0$ [22] consistent with charge transfer from V to TCNE (π backbonding) such that more transferred charge resides near the more electronegative N sites. These results reveal interaction-induced changes in the LUMO of $TCNE^0$ and also imply that its planar geometry and general structure remain intact in $V[TCNE]_{x\sim2}$.

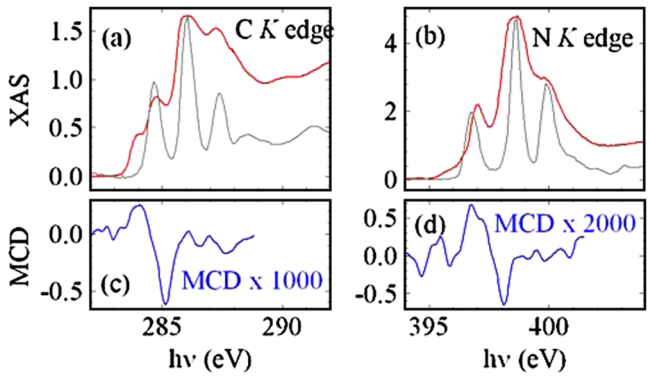

FIG. 3 (color online). C (left) and N (right) XAS and MCD spectra for $V[TCNE]_{x\sim2}$ are in the top and bottom panels, respectively. Scaled XAS spectra from $TCNE^0$ (gray) are included.

MCD is observed at the C and N edges [Figs. 3(c) and 3(d)] providing the first evidence of spin polarization of the $TCNE^{\bullet-}$ π system in $V[TCNE]_{x\sim2}$. Its small size results from weak $2p$ spin-orbit coupling and no spin-orbit splitting in the $1s$ levels, implying that K edge MCD senses only m_l and not m_s [23]. Even with low S/N, distinct MCD is apparent in the lower part of the π^* region where XAS splitting exists. C MCD shows positive and negative peaks at 284 and 285 eV, respectively. N MCD shows positive and negative peaks at 397 and 398 eV, respectively.

Further insight into the $V[TCNE]_{x\sim2}$ electronic structure comes from collecting C, N, and V spectra as in Fig. 4, where each is plotted over a 10 eV range to roughly align E_F for each element. Such alignment is approximate ($\pm$0.5 eV) because of general uncertainty in E_F and different chemical shifts of distinct C and N sites. Even so, clear correlations further support the bonding and backbonding model. The Gaussians in the V XAS spectrum fall just above the former third LUMO in the C and N spectra in the TCNE σ^* region, consistent V σ^* states and explaining their width. Photoemission reveals an enhancement of filled DOS roughly 6 eV below E_F [12] that would correspond to the bonding counterpart of this interaction. The coincidence of specific features in the $TCNE^{\bullet-}$ π^* and the V T_1 spectra is consistent with backbonding interactions.

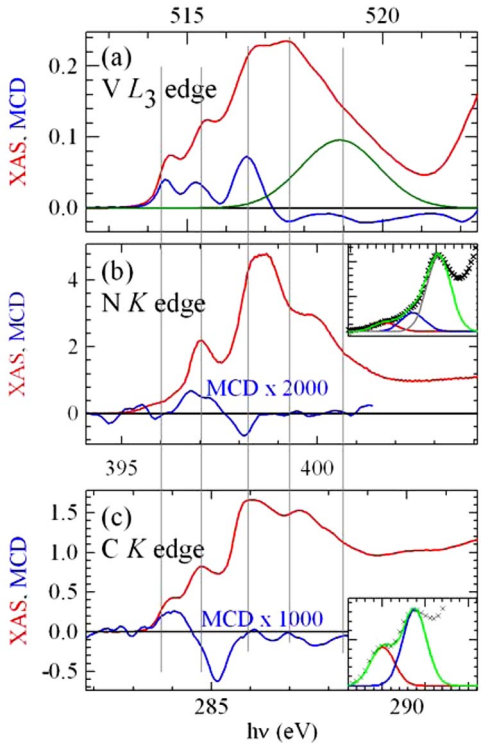

FIG. 4 (color online). XAS (red or gray) and MCD (blue or dark gray) at all three edges in $V[TCNE]_{x\sim2}$, (see text for vertical alignment). Insets in (b) and (c) show Gaussian fits to the low energy XAS regions. (a) Includes the Gaussian representing transitions into σ^* states in the bonding and backbonding model. Vertical lines are visual guides.

In the former first LUMO region in $V[TCNE]_{x\sim2}$, two and three peaks can be resolved at the C and N edges, respectively [Figs. 4(b) and 4(c) insets]. 0.7 eV separates these peaks at both edges. For C this region is dominated by transitions from the central C_1 sites, while for N 2 distinct sites contribute, only 3/4 of which coordinate with V. This multiplicity of N sites explains why three peaks are resolved for N while only two are resolved for C. In Fig. 4 the two split peaks in the C spectrum are aligned to the second and third split peaks in the N spectrum.

The opposite MCD of the two peaks in the C spectrum leads us to consider whether magnetic exchange between V and TCNE accounts for the 0.7 eV splitting. Charge transfer from V to TCNE yields a singly occupied former LUMO that splits into spin-polarized subbands in a magnetic sample. The magnetic exchange energy in $V[TCNE]_{x\sim2}$ [24] is more than 10 times smaller than the observed splitting. Rather than exchange splitting, we note the observed value is of the same order as the V T_1 multiplet splitting. Thus backbonding interactions between relatively unperturbed, spin-polarized V d_{xy}-like states and more strongly perturbed TCNE π^* MO states can account for the former LUMO splitting.

Magnetism and activated transport in $V[TCNE]_{x\sim2}$ are explained by a large imbalance in occupation of spin-split subbands of the $TCNE^{\bullet-}$ former LUMO. $TCNE^{\bullet-}$ spins in the occupied, lower subband align antiparallel to V^{2+} spins in weakly hybridized backbonding levels, yielding ferrimagnetic alignment of $TCNE^{\bullet-}$ and V^{2+} spins. The empty, upper subband is then spin aligned with filled V^{2+} d states at E_F, yielding semiconducting transport with activation energy close to the measured value of 0.5 eV [4,5]. Coulomb repulsion within the π^* levels [4] may contribute to the energy splitting along with hybridization.

While disorder precludes the use of polarized XAS to measure relative orientation of V^{2+} and $TCNE^{\bullet-}$ backbonding orbitals, they are largely predicted by this model. In a reference frame with V^{2+} centered in a cube and the d_{z^2} and $d_{x^2-y^2}$ orbitals pointing to face centers, σ bonding orients one of the four arms of each of the six ligands along three orthogonal V-N-C_2 axes. V d_{xy}-like orbitals point toward cube edge centers, and backbonding interactions with π MOs of a given $TCNE^{\bullet-}$ depend on its azimuthal orientation about its σ bond axis. When its π lobes point toward the cube edge centers they have maximum overlap with d_{xy}-like orbitals, and a given d_{xy}-like lobe overlaps with so-oriented π lobes from 1 or 2 different $TCNE^{\bullet-}$ ligands. Alternatively, π orbitals that align toward the cube corners overlap with two different d_{xy}-like orbitals from the same V^{2+} center. Disorder in this azimuthal degree of freedom yields a range of backbonding interactions broadening the C and N π^* peaks. That this is nonclassical backbonding [25] (the C $\equiv$ N IR stretch [26] shows little redshift) may result from π and π^* delocalization over the entire $TCNE^{\bullet-}$ and the 3D nature of the covalently bonded network.

In summary, combined C, N, and V XAS and MCD reveal bonding and backbonding interactions in $V[TCNE]_{x\sim2}$ that explain its novel electronic properties with a detailed and predictive electronic structure. Strong covalent σ bonding holds V^{2+} and $TCNE^{\bullet-}$ constituents together while weaker π backbonding interactions mediate combined magnetic and semiconducting transport properties. This model can be tested with further x-ray and other experimental studies in this and related systems, and provides a clear starting point for density functional theory studies of material properties and to yield more realistic models of measured x-ray spectra in mixed metal-organic systems in which mixed ionic and covalent bonding limits applicability of atomic models.

Measurements using beam lines 4.0, 8.0, and 6.3.2 at the Advanced Light Source (LBNL) were supported by the Division of Materials Sciences and Engineering, Office of Basic Energy Sciences, under DOE Contract No. DE-AC02-05CH11231. Synthesis and characterization were supported in part by AFOSR Grant No. FA9550-06-1-0175 and DOE Contracts No. DE-FG-02-01ER45931, No. DE-FG02-86ER45271, and No. DE-FG03-93ER455504.

[1] J. S. Miller and A. J. Epstein, Chem. Commun. (Cambridge) 13 (1998) 1319.
[2] A. J. Epstein, MRS Bull. **28**, 492 (2003).
[3] J. M. Manriquez *et al.*, Science **252**, 1415 (1991).
[4] V. N. Prigodin *et al.*, Adv. Mater. **14**, 1230 (2002).
[5] N. P. Raju *et al.*, J. Appl. Phys. **93**, 6799 (2003).
[6] J. W. Yoo *et al.*, Phys. Rev. Lett. **97**, 247205 (2006).
[7] J. W. Yoo *et al.*, Phys. Rev. Lett. **99**, 157205 (2007).
[8] D. Haskel *et al.*, Phys. Rev. B **70**, 054422 (2004).
[9] K. I. Pokhodnya, A. J. Epstein, and J. S. Miller, Adv. Mater. **12**, 410 (2000).
[10] C. Tengstedt *et al.*, Phys. Rev. B **69**, 165208 (2004).
[11] C. Tengstedt *et al.*, Phys. Rev. Lett. **96**, 057209 (2006).
[12] M. P. de Jong *et al.*, Phys. Rev. B **75**, 064407 (2007).
[13] F. de Groot and A. Kotani, *Core Level Spectroscopy of Solids* (CRC Press, Boca Raton, 2008).
[14] P. Frank *et al.*, Inorg. Chem. **41**, 3269 (2002).
[15] T. Mallah *et al.*, Science **262**, 1554 (1993).
[16] W. R. Entley and G. S. Girolami, Science **268**, 397 (1995).
[17] P. Carra *et al.*, Phys. Rev. Lett. **70**, 694 (1993).
[18] Close spacing of V L_3 and L_2 lines hinders separation of m_s and m_l. The ratio m_l/m_s can be determined.
[19] A. Zheludev *et al.*, J. Am. Chem. Soc. **116**, 7243 (1994).
[20] M.-J. Hubin-Franskin *et al.*, J. Chem. Phys. **106**, 35 (1997).
[21] C. I. Oprea, A. Damian, and M. A. Girtu, J. Optoelectron. Adv. Mater. **8**, 191 (2006).
[22] After renormalizing C(N) spectra to have the same edge jump, areas of π^* peaks are proportional to empty π state density.
[23] G. Y. Guo, J. Phys. Condens. Matter **8**, L747 (1996).
[24] A. J. Epstein and J. S. Miller, Mol. Cryst. Liq. Cryst. **233**, 171 (1993).
[25] F. A. Cotton *et al.*, *Advanced Inorganic Chemistry* (Wiley-Interscience, New York, 1999).
[26] J. S. Miller, Angew. Chem., Int. Ed. **45**, 2508 (2006).